A short bibliographic report on Small UAV design

Laura STANESCU[1], Constantin Alexandru MATEI[2]

*Corresponding author
[1]"POLITEHNICA" University of Bucharest, Faculty of Aerospace Engineering,
Gheorghe Polizu St. 1-7, sector 1, 011061, Bucharest, Romania,
alexandra_laura18@yahoo.com
[2]"Alexandru Ioan Cuza" Police Academy of Bucharest, Romania,
Aleea Privighetorilor St. 1-3, sector 1, 014031, Bucharest, Romania,
alexander_ctin@yahoo.com

DOI: 10.13111/2066-8201.2019.11.3.14

Received: 19 March 2019/ Accepted: 01 August 2019/ Published: September 2019

Abstract:*This article presents a detailed example for the design of all aspects of a prototype unmanned aerial vehicle, also dealing with the use of multi-segmented flight control surfaces of these UAV's wings. Adding multiple segments to the UAV wings creates smaller control surfaces. By introducing smaller control surfaces, a wing can make refined adjustments to UAV's performance while airborne. This unique technique brings several benefits, as follows: applying localized correcting forces to the UAV reduces structural deformation, minimizes the drag action due to the control surface actuation, suppresses and controls the structural resonance due to lift forces and vibrational modes, reduces the weight of the structure, and improves the endurance of flight by using the solar cell.*
This study is a part of a more comprehensive work for my Ph.D. thesis which proposes the construction of a UAV prototype equipped with a solar propulsion system. This system meets the requirements of missions specific to the Ministry of Internal Affairs: both the autonomy capabilities and the performance of the communication systems on and off the ground.

Key Words: *UAV, solar, aerodynamic design*

1. INTRODUCTION

Unmanned aircraft systems (UAS) play an increasing ROLE in defense programs and defense strategy around the world. Technology advancements have enabled the development of large and smaller increasingly capable unmanned aircraft. As recent conflicts have demonstrated, there are numerous military applications for unmanned aircraft, including reconnaissance, surveillance, battle damage assessment and communications relays.

The term "miniature air vehicle", denoted with the acronym MAV1, will be used to refer to the class of fixed-wing aircraft with wing spans less than 5 feet. MAV are typically battery powered, hand launched and belly landed, and therefore do not require a runway for takeoff or landing. They are designed to operate from 20 minutes to several hours. Payloads range from ounces to several pounds. The small payload severely restricts the sensors that can be placed on MAV and also restricts the computer that can be embedded on board. These restrictions pose interesting challenges for designing autonomous modes of operation. While many of the concepts described also apply to larger unmanned aircraft and smaller micro air

vehicles, the primary focus is on the challenges that are inherent in guiding, controlling limited-payload and increasing autonomy for small and miniature aircraft systems.

The first step in aircraft designing, was to perform a feasibility study by identifying existing UAV with similar geometry, size and mission requirements. Using available data from the existing UAV, a parametric study was performed to determine an initial wingspan, power requirement and UAV maximum speed. Fig. 1 illustrates the geometry of the UAV study.

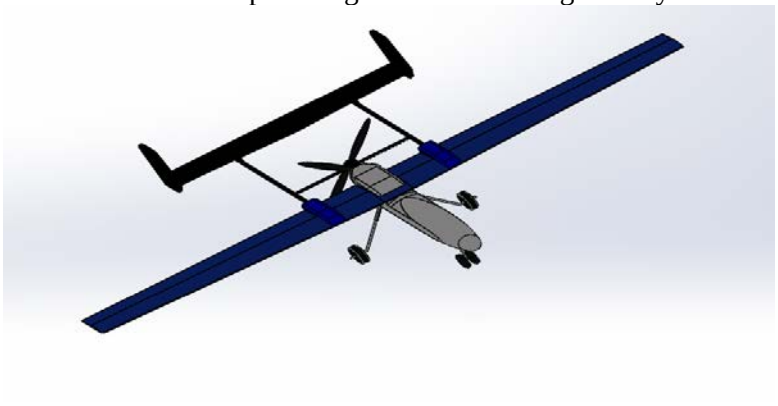

Fig. 1 - The UAV

2. AERODYNAMIC DESIGN PROCESS

The traditional aerodynamic analytical was utilized for developing the aerodynamic UAV model by the following steps:

1. Make sections such as pusher or puller, the span, location of wings relative to each other and chord length;
2. Perform analysis on the geometry of the airfoils selected for the aircraft. One the geometry of the aircraft is selected; it is possible to estimate life-to-drag ratios, static margin, and performance capabilities. The degree of refinement begins to reveal the cost of construction and the types of manufacturing techniques that will be required. This is the approach that was used to design and manufacture the UAV[3];
3. Use the Athena Vortex Lattice (AVL) computational fluid dynamics software package to model the aerodynamic characteristics of the proposed UAV structure;
4. Comparison of chosen aerodynamic characteristics should provide baseline aerodynamic parameters for state-space model to be used in the development of an autonomous controller [3].

Following the steps mentioned above allows for the completion of the UAV design.

For the UAV design, a decision must be made between increasing the maneuverability or the stability of the aircraft. For the aerodynamic design of our UAV, priority was given to an increase in stability and payload rather than an increase in maneuverability. To achieve this, a twin boom pusher assembly with a rectangular wing was selected.

2.1 Geometry and configuration

The UAV design has a rectangular main wing with a wingspan of 1,68 m, a mean aerodynamic chord of 0.32 m and an aspect ratio of 6,76. In order to simplify the design and analysis, the main wing does not change geometry along its span nor is it swept. The aircraft is estimated to have a gross weight of 5 kg. The airfoil selected for the main wing is an NACA 3316, and the airfoil type were selected so that the UAV will exhibit a high lift at low speeds and provides

adequate moments for stable pitch. Other aircraft specifications are shown in Tables 1-3 below. The control surface sizing was based on the results of the stability studies conducted in AVL. Based on the results, the sizes of the control surfaces for the aircraft are shown in Table 4 below.

Fig. 2 shows a representation of the UAV main geometry which includes the main wing and the horizontal and vertical tails. The mauve areas represent the control surfaces.

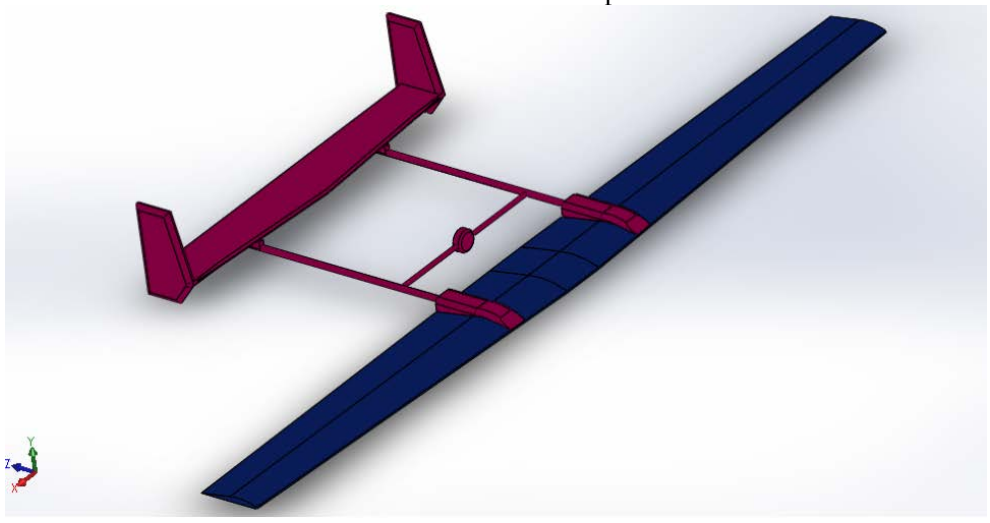

Fig. 2 - Representation of UAV geometry and control surface

2.2 Airfoil section

This section describes the process in determining the final geometry of the UAV based on the CFD analysis and empirical calculation. As mentioned in the previous section, the airfoil type was selected so that the UAV will exhibit a high lift at low speeds and provides adequate moments for stable pitch.

Several experimental studies were performed in order to identify the final airfoil selection for the wing and horizontal tail/vertical tail.

The airfoil types for these wing and tail combinations included in these studies were the Eppler 214 and NACA 0012, Clark Y and NACA 2412, Eppler 214 and NACA 2412.

The E 214 and CLARK Y were chosen for the main wing, while the NACA 0012 and NACA 2412 were chosen for the horizontal and vertical tail.

Since the interaction of the wing and tail is vital for the performance of the aircraft, the airfoil selection was based on the following design criteria:

- Lift/Drag (L/D) must be greater than 15;
- Good trim conditions (which implies good pitch stability).

Table 1 - Wing specifications

Wing (airfoil)	NACA 0012
Weight	1,53 kg
Wing loading	6.71 kg/m^2
Aspect ratio	6.76
Taper ratio	2.169
Wing area	0.399 m^2
Wingspan	1.68 m
Root chord	0.15

Tip chord	0.325
Average chord length	0.309
Quarter chord sweep angle	$L=0^0$
Leading-edge sweep	$L=0^0$
Span efficiency	0.248
Thickness ratio	16%

Table 2 - Horizontal stabilizer

Horizontal stabilizer (airfoil)	NACA E 214
Span	0.59 m
Root chord	0.104
Tip chord	0.181
Average chord length	0.297
Planform area	0.104 m^2
Taper ratio	0.181
Aspect ratio	3.351

Table 3 - Vertical stabilizer

Vertical stabilizer (airfoil)	NACA 2412
Span	0.12 m
Root chord	0.094
Tip chord	0.102
Average chord length	0.102
Planform area	0.12 m^2
Taper ratio	11
Aspect ratio	1

Table 4 - Control surface specification

	Flaps	Aileron	Elevator	Rudder
Chord (m)	0.14	0.14	0.091	0.99
Span (m)	0.762	0.508	1.64	0.609

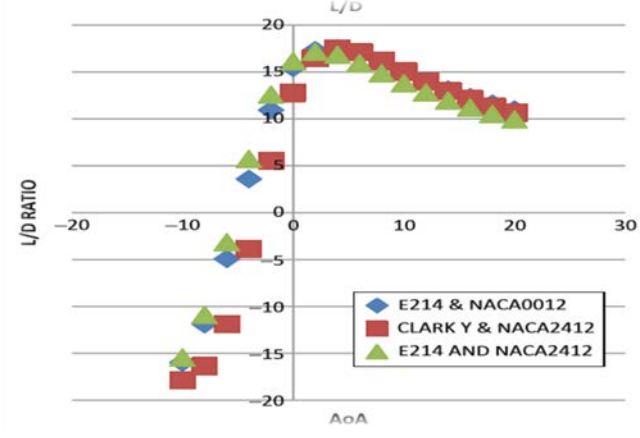

Fig. 3- Angle of attack versus lift-to-drag ratio

Fig. 3 shows the different lift-to-drag ratios for the selected airfoil combinations, and all performed with an L/D ratio greater than 15 (value Lift/Drag - the following design criteria). Fig. 4 which shows the pitch stability of the aircraft combinations. It can be seen that NACA

2412, CLARK Y and NACA 0012 have negative pitch stability. Since the objective of the UAV is to be naturally stable during steady flight, this negative pitch stability is not desired. The selected airfoil combination provided the most desired performance for the main UAV was the NACA 0012 for the main wing and the E 214 and CLARK Y for the tail. The final set of experiments for this study was to evaluate the drag performance of the different airfoil combinations. Fig. 5 demonstrates that the E 214 and NACA 00012 combination has the lowest drag [3-5].

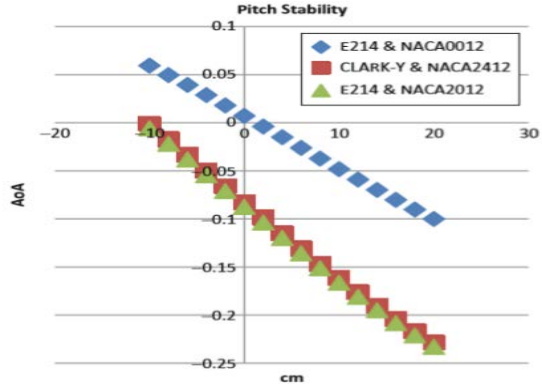

Fig. 4- Pitch stability

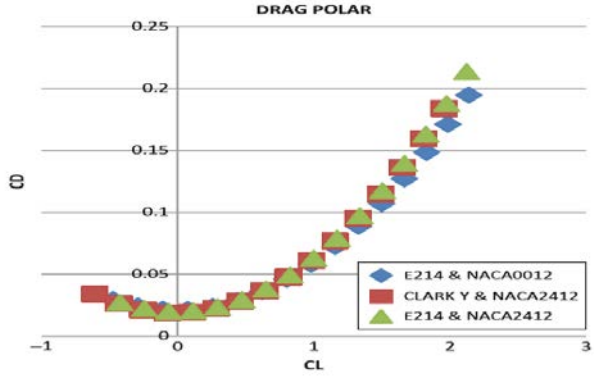

Fig. 5 - Drag polar

Based on the analysis that was performed, the optimal airfoil combination selected for the UAV was the NACA 00012 since this combination provides (1) optimal L/D, (2) the lowest drag polar and (3) the most stable aircraft performance. Table 5 below shows the aerodynamic data obtained from both empirical studies and CFD analysis.

Table 5 - Aerodynamic coefficients from empirical studies

Skin friction coefficient	C_{fe}
Zero lift parasite drag coefficient	C_D
Span efficiency	e
Induced drag factors	K_1
	K_2
	K_3
	K
Propulsion efficiency	Ŋ=0.70

Total power available	P
Speed	V=83.56
Max curve slope	CL_{max}=1.06
Stall speed	V_{stall}= 49.89
Maximum lift-to-drag ratio	L/D= 18.8

These coefficients are determined from both analytical and CFD analysis using AVL. The AVL software uses the vortex lattice method to estimate the lift and drag forces on the modeled aircraft. This software package was used during the design of the UAV to ensure that the design provided adequate lift for both the UAV structure and the 14lb payload.

The software was also used to determine aircraft stability and to provide other necessary aerodynamic parameters.

The CFD study also determined that the wing and the horizontal tail must have an incidence angle of 2º. The necessary angles of attack for the main wing were found by optimizing the lift-to-drag ratios at cruising conditions.

In addition to this, AVL was used to perform studies to investigate the overall performance of the aircraft at different speeds and altitudes.

Optimizing an aircraft design minimizes fuel consumption, minimizes drag, and reduces the loads that the structure experiences. By applying CFD to an aircraft design, performance of the UAV design can be simulated.

The simulated performance can be used to determine if off-the-shelf components, such as an engine, can be used while maintaining design parameters of the aircraft. If off-the-shelf parts can be utilized rather than custom parts, both time and cost of manufacturing are reduced. For the UAV, the simulation showed that an off-the-shelf engine met the aircraft requirements and a Desert Aircraft model DA-120 engine was purchased.

Another important parameter in aircraft design is the static margin. This is the distance between the neutral point (i.e., the entire aircraft's aerodynamic center) and the center of gravity divided by the length of the chord.

The static margin is used in determining the longitudinal stability of an aircraft. A positive static margin on an aircraft means that the center of gravity is in front of the neutral point, while a negative static margin on an aircraft means that the center of gravity is behind the neutral point.

As the static margin increases, the longitudinally stability increases. However, as the static margin increases, maneuverability decreases. As stated previously, the stability on the mine UAV was determined to be more important that its maneuverability, so this UAV was designed with a static margin of 16% [1], [5-8], [9-12], [14].

3. STRUCTURAL REQUIREMENTS

The flight operating strength of a UAV is presented in Fig. 6 whose horizontal scale is airspeed (V) and vertical scale is load factor (n). This diagram is made for operated UAV, to prevent structural damage and ensure that the anticipated service life of the airplane is obtained.

The structural design of a UAV is based on the aerodynamic loads generated during each stage of the mission which include takeoff, climb, cruise, diving, and landing [1], [9], [14].

Fig. 6 resulted from the mathematical results obtained during each stage of the mission, including take-off, cruise, sinking and landing, which were implemented for the calculation of the flight envelope.

The results used to obtain the flight envelope are experimental, not after the UAV operation.

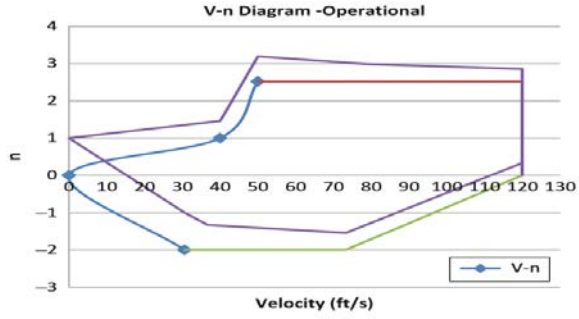

Fig. 6 – Flight envelope

These loads are determined from CFD and from the flight envelope of the mine UAV as seen below in Fig. 6. Based on the maneuverability requirements of the UAV design, the maximum acceleration loading was set to 3g. This is the largest acceleration that UAV will experience in the flight envelope. Thus, the aircraft structure was designed to meet the 3 g loading condition while maintaining a factor of safety of 2. Initial weight estimates obtained from a finite element model (FEM) indicate that an aircraft structural designed to meet these loads would weigh approximately 5 kg.

3.1 Engine section

An electric motor uses electrical energy to produce mechanical energy. This definition is very general and in fact there exists a very large variety of electric motors that coexist because of the different supply sources, sizes, torques and speeds depending on the application. In the present case, DC (Direct Current or Continuous Current) motors will be used as they are designed to run on DC electric power supplied by a battery. By far the most common types are the brushed and brushless types, which use mechanical and electronic commutation, respectively, to create a rotating magnetic field vector that pulls an electromagnet or a permanent magnet. In a classic DC motor, the inner part is the rotor, which consists of a wound coil generating a rotating magnetic field, and the outer part is either an electromagnet or permanent magnet stator, which creates a fixed magnetic field [13].

The drive electronics is more complex that for brushed motors because it has to activate the coils one phase after the other that has to be synchronized to the rotor's position. In order to sense the position, either Hall Effect sensors or Back Electro Magnetic Force (BEMF) are used. When configured with the magnets on the outside, they are referred to as out runner motors, else they are called in runner. The advantages of BLDC motors are numerous: very precise speed control, high efficiency, reliability, reduced noise, longer lifetime (no brush abrasion), and no ionizing sparks. Additionally, they run much cooler than brushed motors which allows the use of higher currents.

3.2 Composite stress analysis

The structure's margin of safety was determined utilizing the Tsai-Hill Failure Index (FI) to predict the failure in composite materials. The FI is defined as

$$FI = \frac{\sigma_1^2}{X^2} - \left(\frac{1}{X^2} + \frac{1}{Y^2} + \frac{1}{Z^2}\right) * \boldsymbol{\sigma_1\sigma_2} + \frac{\sigma_2^2}{Y^2} + \frac{\sigma_{12}^2}{S^2} \qquad [15] \qquad (1)$$

$\boldsymbol{\sigma}_1$ = calculated plane stress of the sandwich panel in direction 1,
$\boldsymbol{\sigma}_2$= calculated plane stress of the sandwich panel in direction 2.

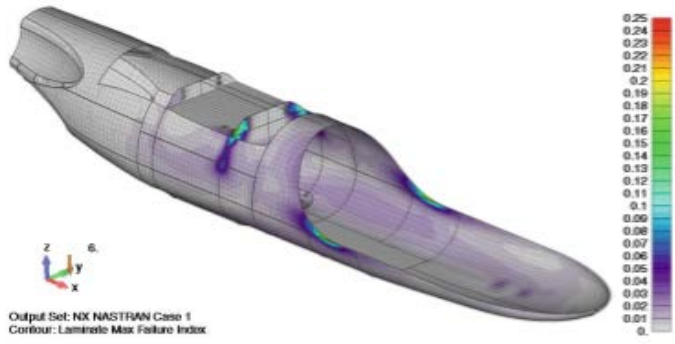

Fig. 7 - Fuselage stress contours

τ_{12} = calculated in-plane shear stress of the sandwich panel,
X = normal allowable stress of the sandwich panel in the X direction,
Y = normal allowable stress of the sandwich panel in the Y direction,
Z = normal allowable stress of the sandwich panel in the Z direction,
S = in-plane shear allowable of the panel.

3.3 Modeling

All internal loads were applied using mass element when the laminate properties of the fuselage skin, bulkheads, and internal components were modeled [3]. All mass elements are attached to the structure using interpolation elements in FEM model.

That force can be considered as a "force link", which distributes the forces of the independent nodes to the dependent nodes by interpolation. The fuselage structure load was applied by specifying the aircraft accelerations in the FEA model, as seen in Fig. 7. An engine thrust load of 0.045 kg was also applied to the engine assembly mass element and the fuselage was co-trained at the interface between the bulkheads and the main spar of the wing.

The structure of the wing-boom-tail assembly and all internal ribs were modeled using the laminate properties.

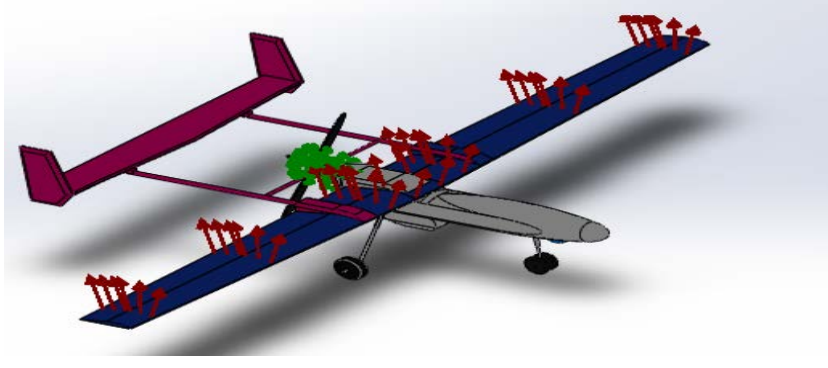

Fig. 8 - FEA analysis of wing structure

For the wing-boom-tail assembly (Fig. 8), all lift loads were applied using nodal loads. A distributed lift load, which decreased toward the wing and tail tips, was calculated by incorporating a maximum gust load of 3.0 g and the aircraft accelerations obtained from the FEA (Finite Element Analysis that is a simulation program) model. The wing is constrained

at the interface between the bulkheads of the fuselage and the main spar of the wing. Fig. 8 shows the main load-bearing structure within the wing which is a composite spar that has a box beam configuration. The spar is composed of alternating layers of both bidirectional and unidirectional carbon fiber. The layers of unidirectional carbon fiber are orientated in the spanwise direction to maximize the tensile and compressive strength of the carbon fiber in bending. The bidirectional layers of carbon fiber are orientated in a 45 angle with respect to the spanwise direction to increase the strength of the spar under torsional loading. Regions where the spar experiences the least bending moments are manufactured with fewer layers of carbon fiber. The loading transferred from the tail through the booms add additional local stresses. To alleviate large stress concentrations, the spar and local sandwich panels were reinforced with additional layers of carbon fiber. The base main wing was optimized and reinforced by increasing the number of layers of carbon fiber to counteract the large bending moments experience near the root chord. As the bending moment decreases with distance from the root, the number of layers of carbon fiber is decreased to prevent the risk of peak stress concentrations. Based on previous structural analysis, additional reinforcement was required in regions where the central wing, the wing tip extensions, and the booms connect.

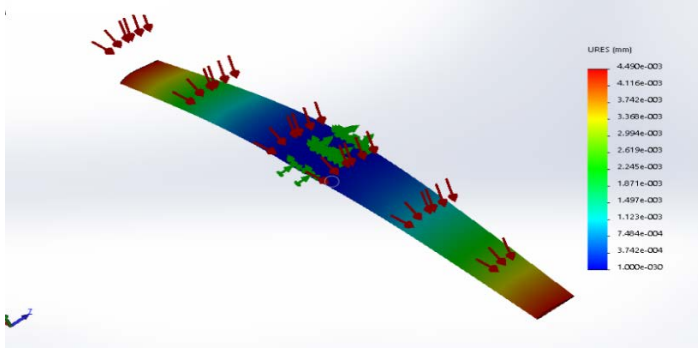

Fig. 9 - Simulated deflections caused by in-flight loads

The results of the FEM (Finite Element Method) show that the aircraft in a 3.0 g maneuver is capable of withstanding an ultimate aerodynamic load of 6.89 kg and can have expected wing tip deflections up to approximative 0.011086 m (4,490 e -0,03) (Fig. 9).

Normal Mode Shapes and Mode Frequencies

A structure modal analysis must be performed since uncontrolled vibrations can be catastrophic for the aircraft [2]. Based on the finite element modeling shown in Fig. 10, the first structural bending mode frequency of the UAV main wing was determined to be 5Hz.

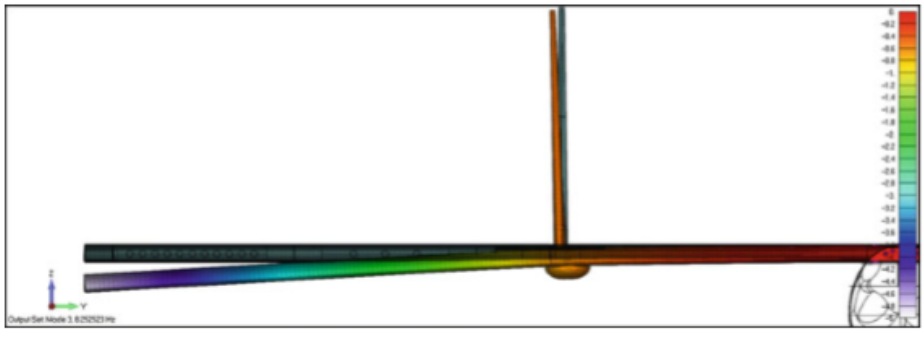

Fig. 10 - Analysis of the first structural bending mode frequency

Stress and Strain

The FEM of the UAV wing-boom-tail was used to predict the stress and strain fields in the structure while under load. The greatest stress concentration occurs near the root of the wing, while the peak stress concentration occurs near where the fuselage attaches to the wing (Fig.10). The direction of composite material needs to be specified during manufacturing [2]. The skin material used in the UAV is a bidirectional carbon fiber weave which has equal stiffness and strength in two directions. However, the spar is composed of unidirectional carbon fiber, which is stiffer and stronger in the tow direction. FEM allows the user to specify the tow direction of the composite material. Since the largest contribution to stress on the wing structure is due to bending, it is critical to analyze the strain contours in the wingspan direction (Fig. 11).

Computational Fluid Dynamics

The Athena Vortex Lattice was used as the CFD software to calculate the aerodynamic parameters and the flight dynamics of the UAV. It is a free resource software package that is an effective tool to approximate and refine the flight dynamic characteristics of a custom-built rigid-body UAV. The two major approximations made by the Athena Vortex Lattice include the following: the software treated the fuselage as a slender body and did not consider certain drag features (booms and the main landing gear) of the UAV model, and the software used an average skin friction drag coefficient. The actual skin friction drag coefficient requires extensive wind tunnel testing and it typically makes a small contribution to the overall drag coefficient of the aircraft. Regardless of these approximations, the software can provide a reasonable aerodynamic model that can be refined from flight testing.

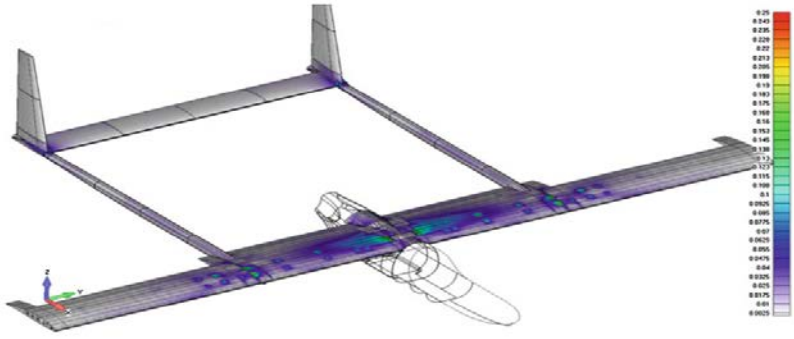

Fig. 11 - Wing assembly stress contours

6. CONCLUSIONS

This paper has presented a rationale for the UAV designer, to choose an aircraft configuration and a methodology for sizing it. By iteratively changing such aircraft configuration parameters as wing aspect ratio and camber, the designer can determine the smallest/cheapest UAV that can meet the design mission. This process is one way to optimize UAV designs for maximum performance and minimum size/cost.

The chosen construction solution proved to be a very good decision, certified by the results of calculations and simulations performed.

This solution can be implemented on a real prototype, design of the avionic system, controller implementation via simulation and component fabrication and implementation.

Finally, performance will be evaluated, tested and confirmed with real flight missions.

Stability analysis should be performed to determine whether the aircraft has any uncontrollable, unobservable or unstable modes, once the model has been derived.

In this paper all performance parameter calculations, analysis and parts selection are discussed. This type of aircraft can be used to fly both day and night. Main advantage of its use is the non-conventional source of energy. As discussed in paper, the dimensions and number of solar cell are of the specified type. We will continue with the effective design of the aircraft and the location of the solar propulsion system on the UAV. After testing it, we will make modifications as per requirement and those experimental results will be published later in a future edition of the bulletin.

REFERENCES

[1] J. D. Anderson Jr., *Aircraft Performance and Design*, McGraw Hill, Boston, pp. 32-56, 1999.
[2] A. Derkevorkian, J. Alvarenga, J. Bakalyar, L. Richards, S. Masri, H. Boussalis, *Evaluation of strain-based deformations hape estimational gorithms for control and monitoring applications*, in 2012 SPIE Symposium on SPIE Smart Structures and Materials Nondestructive Evaluation and Health Monitoring, San Diego, pp. 12-70, March 2012.
[3] M. Niță, *Avioane și rachete. Concepte de proiectare*, Ed. Militara, București, 1985.
[4] I. Grigore, *Mecanica zborului avionului*, pp. 65-78, Ed. Academia Militară, București, 1987.
[5] J. D. Anderson Jr., *Fundamentals of aerodynamics*, Ed. McGraw-Hill, 2005.
[6] W. Shy, Y. Lyan, D. Viieru, *Aerodynamics of low Reynolds number flyers*, Ed. Cambridge, pp. 45-48, 2004.
[7] I. Sălageanu, *Aerodinamica vitezelor subsonice*, Vol.**I**,**II**, Ed. Academia Militară, București, 1981.
[8] V. Avădani, *Calculul Avionului la Rezistență*, Ed. Academia Militară, București, 1976.
[9] D. Lee, M. Mitrovich, A. Friedman, G. Carman, L. Richards, Characterization of fiber optic sensors for structural health monitoring, *J. Compos. Mater.*, **36**(11), pp. 1349-1568, 2002.
[10] D. P. Raymer, *Aircraft Design: A Conceptual Approach*, AIAA Education Series, 3rd edn., AIAA, Reston, 1999.
[11] W. Ko, W. Richards, *Method for real-time structure shape-sensing*, pp. 1–13, Apr 2009.
[12] W. Ko, W. Richards, V. Tran, *Displacement Theories for In-Flight Deformed Shape Predictions of Aerospace Structure*, National Aeronautics and Space Administration (NASA), pp. 214-612, 2007.
[13] T. H. G. Megson, *Aircraft Structures for Engineering Students*, pp. 123-156, 1999.
[14] N. L. Robert, *Machine Design An Integrated Approach*, Prentice Hall, Upper Saddle River, 2006.
[15] * * * https://apps.dtic.mil/dtic/tr/fulltext/u2/a216600.pdf